Theoretical and Applied Mechanics Letters 12 (2022) 100346

Contents lists available at ScienceDirect

Theoretical and Applied Mechanics Letters

journal homepage: www.elsevier.com/locate/taml

Letter

Design of elliptical underwater acoustic cloak with truss-latticed pentamode materials

Yuanyuan Ge, Xiaoning Liu*, Gengkai Hu

School of Aerospace Engineering, Beijing Institute of Technology, Beijing 100081, China

ARTICLE INFO

Article history:
Received 10 April 2022
Revised 20 May 2022
Accepted 23 May 2022
Available online 27 May 2022

Keywords:
Elliptical acoustic cloak
Pentamode material
Microstructure design
Truss lattice

ABSTRACT

Pentamode acoustic cloak is promising for underwater sound control due to its solid nature and broadband efficiency, however its realization is only limited to simple cylindrical shape. In this work, we established a set of techniques for the microstructure design of elliptical pentamode acoustic cloak based on truss lattice model, including the inverse design of unit cell and algorithms for latticed cloak assembly. The designed cloak was numerically validated by the well wave concealing performance. The work proves that more general pentamode acoustic wave devices beyond simple cylindrical geometry are theoretically feasible, and sheds light on more practical design for waterborne sound manipulation.

Invisible cloaks and other devices aiming to freely manipulate physical fields have been fascinating subjects these years. Pendry et al. [1] and Leonhardt [2] first came up with the concept of transformation electromagnetics (EM), based on the pioneering work of Dolin [3], and the EM cloak was soon demonstrated with metamaterial techniques [4]. Transformation acoustics based on metafluid of anisotropic density was first proposed by observing the analogy between acoustic equation and Maxwell's equation [5,6]. A variety of meta-fluids realizing anisotropic density have been suggested, such as alternating fluid layers, perforated plates immersed in fluid, etc., however the working media are basically fluidic in nature [7–9].

Besides the meta-fluids with anisotropic mass density, there is however an alternative route for acoustic cloak making use of solid-based pentamode material (PM) with anisotropic modulus. PM is degenerated elastic material with elastic tensor having a single nonzero eigenvalue [10]. By microstructure design, PM can support a more general stress state other than the hydrostatic of conventional fluids [11–13]. The milestone for transformation acoustics based on PM is due to Norris, he proved that, under curvilinear coordinate transformation, conventional acoustic equation possesses the same form as that of PM wave equation [14]. Acoustic cloak using PM has advantages of broadband efficiency and solid nature, thus is more promising for practical applications. These merits stimulated intense researches on PM transformation acoustics and a number of wave manipulation functions have been designed and experimentally demonstrated for underwater sound [15–19]. It is worth mentioning that some active schemes have been successfully used in elastic waves steering and wideband cloaking [20,21], whether these active techniques could be employed in tuning solid materials towards desired PM behavior for waterborne acoustic control is also an interesting problem.

At present, design of PM acoustic devices was mostly limited to regular configurations. The origin is that, in accordance with the divergence-free characteristic stress of the graded PM, the coordinate mapping must be curl-free in order to produce a symmetric deformation gradient tensor [22]. This requirement is only easy to achieve with axisymmetric shape such as the cylindrical and the spherical cloak. By interpreting the mapping as displacement field of a special elastostatic problem, Chen et al. [22] proposed a solution to construct quasi-curl-free mapping for arbitrary shaped PM cloak, with which PM properties for irregular cloak can be obtained. Recently, Quadrelli et al. [23] derived quasi-curl-free mapping as well as the necessary PM properties for a double-elliptical cloak making use of the elliptic coordinates. However, microstructure design of cloak other than cylindrical shape is not reported so far. In comparison with the asymmetric cloak, an essential difference is that the PM unit cell must be designed and assembled cell by cell and no preferred orientation can be presupposed, thus necessitating substantial updating of design techniques. PM based acoustic wave control, though possessing much advantages over other metafluids, their engineering applications would be quite limited if the device configuration can only be cylindrical or spherical. The techniques devised in this work will be very meaningful for extending PM based wave functionality to applications with

* Corresponding author.
E-mail address: liuxn@bit.edu.cn (X. Liu).

https://doi.org/10.1016/j.taml.2022.100346

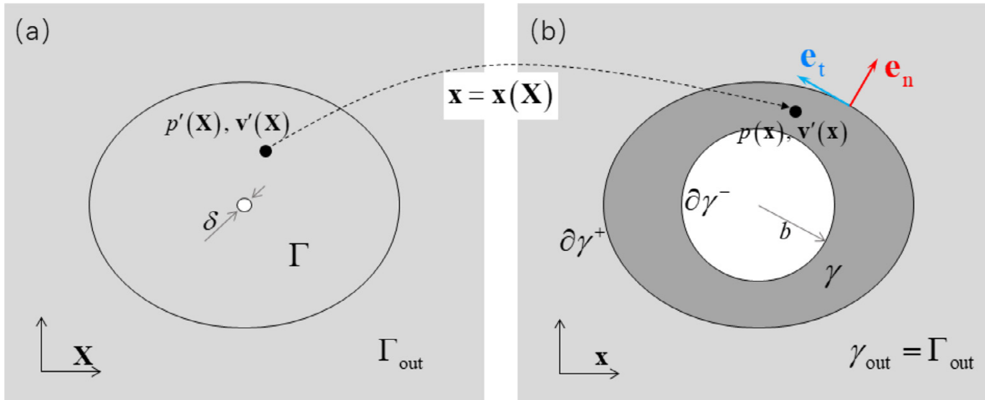

Fig. 1. Illustration of transformation acoustics based on PM material: **a** Virtual space; **b** Physical space.

general geometry, e.g. cloaking of irregular underwater vehicles, arbitrary wave bender, carpet cloak, etc.

In this letter, we will present a systematic microstructure design scheme for an elliptical PM cloak based on ideal truss lattice model [24]. The algorithm proposed in Ref. [22] is adopted at first to determine the required gradient PM distribution for a typical elliptical cloak. Then analytical homogenization of PM for a general unit cell is given in closed form, with which efficient inverse design of PM cell can be implemented. Finally, algorithms are established to segment the cloak domain and to assemble the PM cells up to an integral latticed cloak. The performance of the designed cloak will be numerically validated via finite element simulation.

Gradient PM properties for an elliptical cloak

PMs are characterized by elastic tensor with only one nonzero eigenvalue, hence the elastic tensor can be expressed as $\mathbf{C} = K\mathbf{S} \otimes \mathbf{S}$ [10,14], where the second order symmetric tensor $\mathbf{S}$ is called characteristic stress. The constitutive relation then reads:

$$\boldsymbol{\sigma} = \mathbf{C} : \boldsymbol{\varepsilon} = K\mathbf{S}(\mathbf{S} : \boldsymbol{\varepsilon}). \tag{1}$$

The material can only withstand stress $\boldsymbol{\sigma}$ proportional to $\mathbf{S}$, i.e., $\boldsymbol{\sigma} = -p\mathbf{S}$, and p is called pseudo pressure in analogy to the acoustic pressure in ordinary fluids. Expressed in pseudo pressure, wave equations of PMs are

$$\mathrm{i}\omega p = K\mathbf{S} : \nabla\mathbf{v}, \mathrm{i}\omega\mathbf{v} = \boldsymbol{\rho}^{-1} \cdot \mathbf{S} \cdot \nabla p, \tag{2}$$

where $\mathbf{v}$ is the particle velocity, ρ the density, and time harmonic convention $\exp(-\mathrm{i}\omega t)$ is adopted. Note that the $\mathbf{S}$ tensor has to be divergence free, i.e., $\nabla \cdot \mathbf{S} = 0$, in order that the material has to be at equilibrium [14]. For the trivial isotropic case of $\mathbf{S} = \mathbf{I}$, Eq. (2) reduces to the traditional acoustic wave equation.

Basic ingredients of transformation acoustics via PM are outlined here in brief with an example of elliptical cloak, as depicted in Fig. 1. Consider a virtual space $\mathbf{X}$ occupied by homogeneous acoustic fluid with density ρ_0 and bulk modulus K_0, pressure $p'(\mathbf{X})$ and velocity $\mathbf{v}'(\mathbf{X})$ are governed by

$$\mathrm{i}\omega p' = K_0 : \nabla_{\mathbf{X}}\mathbf{v}', \mathrm{i}\omega\mathbf{v}' = \rho_0^{-1}\nabla_{\mathbf{X}}p', \tag{3}$$

where $\nabla_{\mathbf{X}}$means gradient with respect to the virtual space coordinates. Two adjacent domains Γ and Γ_{out} sharing an elliptical boundary are identified. A tiny circular void with radius δ is introduced at the center to avoid cloak material singularity. Consider a coordinate transformation $\mathbf{x} = \mathbf{x}\ (\mathbf{X})$ which deforms the virtual space to physical space as shown by Fig. 1b. The mapping keeps Γ_{out} unchanged ($\gamma_{\text{out}} = \Gamma_{\text{out}}$) and squeezes Γ to an elliptical cloak shell γ with a large circular void with radius b. It has been proved that [22], besides the geometry, the physical fields are also mapped to the physical space as$\mathbf{v}(\mathbf{x}) = J^{-1}\mathbf{S}^{-1} \cdot \mathbf{F} \cdot \mathbf{v}'(\mathbf{X})$ and $p(\mathbf{x}) = p'(\mathbf{X})$, provided that the symmetric $\mathbf{S}(\mathbf{x})$ is divergence free. The mapped fields in physical space satisfy wave equations in exactly the same form with those of PMs, i.e. Eq. (2). However, material properties inside the cloak are distributed as

$$\boldsymbol{\rho}^{-1} = \rho_0^{-1}J^{-1}\mathbf{S}^{-1}\mathbf{F}\mathbf{F}^{\mathrm{T}}\mathbf{S}^{-1}, K = K_0J, \tag{4}$$

where $\mathbf{F} = \partial\mathbf{x}\ /\ \partial\mathbf{X}$ is the deformation gradient tensor, and $J = \det\mathbf{F}$.

There is an additional condition for $\mathbf{S}$ at the outer boundary of the cloak required by fields continuity and $\mathbf{S} = \mathbf{I}$ in γ_{out}. At $\partial\gamma^+$, principal directions of $\mathbf{S}(\mathbf{x})$ must be in parallel with the normal and tangent directions ($\mathbf{e}_\text{n}$, $\mathbf{e}_\text{t}$, see Fig. 1b) of the boundary and its normal components must be unity, i.e., $\mathbf{S} = \mathbf{e}_\text{n}\mathbf{e}_\text{n} + S_{\text{tt}}\ \mathbf{e}_\text{t}\mathbf{e}_\text{t}$. So far, there is no general method for constructing divergence free $\mathbf{S}(\mathbf{x})$ under these stringent constraints. One solution is to find a *curl-free* coordinate mapping such that $\mathbf{F} \approx \mathbf{F}^{\mathrm{T}}$ and let $\mathbf{S} = J^{-1}\mathbf{F}$, then $\mathbf{S}$ is nearly symmetric and naturally divergence free because of the identity$\nabla \cdot (J^{-1}\mathbf{F}) = 0$, and the boundary constraint is automatically satisfied. An extra benefit of this choice is that, c.f. Eq. (4), the tensorial density reduces to isotropic one, $\boldsymbol{\rho} = \rho\mathbf{I}$. In this case, the graded PM properties in the cloak shell can be summarized as,

$$\rho(\mathbf{x}) = J^{-1}\rho_0, \mathbf{C}(\mathbf{x}) = \mathbf{S} \otimes \mathbf{S}, \mathbf{S} = \sqrt{\frac{K_0}{J}}\mathbf{F}. \tag{5}$$

Note that here and henceforth, the scalar coefficient is absorbed into $\mathbf{S}$ in the expression of $\mathbf{C}$. If such material pattern could be implemented, the cloak will conceal objects in the cavity and resulting scattering would in theory be the same with that in the virtual space.

Curl-free coordinate mapping can only be constructed intuitively for the cylindrical and spherical cloak. Here for the elliptical cloak, a numerical scheme proposed in Ref. [22] for finding quasi-curl-free mapping for irregular geometry is employed. Define inverse mapping $\mathbf{X}(\mathbf{x})$=$\mathbf{x}$+$\mathbf{u}(\mathbf{x})$ where $\mathbf{u}$ represents displacement taken a point $\mathbf{x}$ back to its corresponding point $\mathbf{X}$ in the virtual space. Thus, $\mathbf{u}$ is prescribed at the inner and outer boundaries of the cloak:

$$\mathbf{u} = 0 \quad \text{on} \quad \partial\gamma^+; \mathbf{u} = (\delta/b - 1)\mathbf{x} \quad \text{on} \quad \partial\gamma^-. \tag{6}$$

Once $\mathbf{u}$ is determined $\mathbf{F}$ can be calculated as $(\partial\mathbf{X}\ /\ \partial\mathbf{x})^{-1}$, and it is obvious that $\mathbf{F}$ is symmetric if $\nabla \times \mathbf{u} = \mathbf{0}$. Though strictly curl-free $\mathbf{u}$ is hardly to get, it has been proved that quasi-curl-free $\mathbf{u}$ field can be obtained by solving

$$\nabla \times (\nabla \times u) = \xi\nabla(\nabla \cdot u), \tag{7}$$

where $|\xi| \ll 1$, in conjunction with the boundary conditions Eq. (6). Actually, Eq. (7) is equivalent to the elastostatic equation of

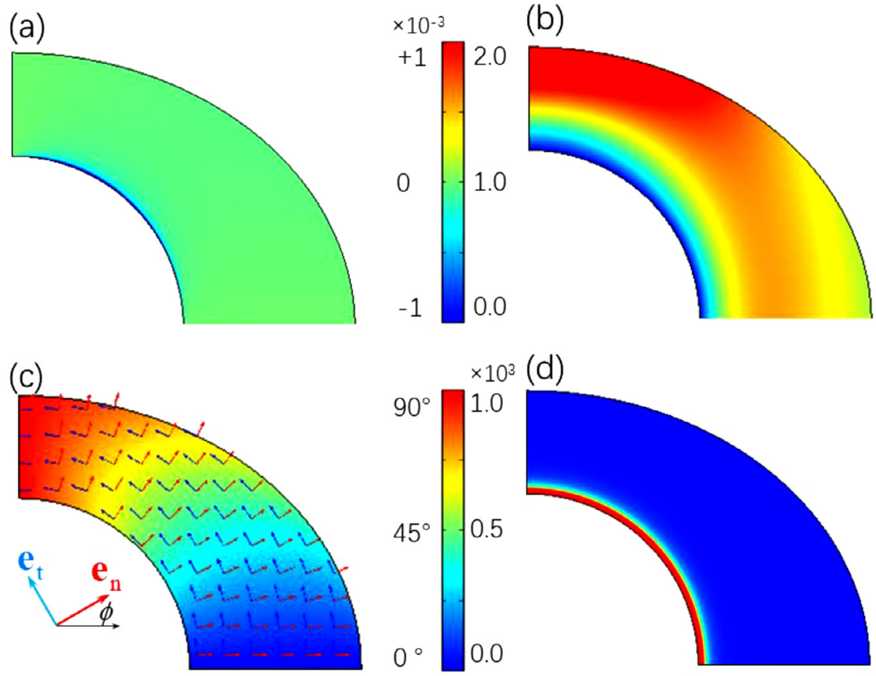

Fig. 2. Contour plots of cloak properties: **a** Symmetry deviation of **F** (F_{12} - F_{21}); **b** Normalized density ρ/ρ_0; **c** Principal orientation angle of **S; d** Anisotropy degree S_t/S_n.

isotropic elastic material with special chosen Lamé constants satisfying $\lambda = (\xi - 2)\mu$, which can be solved easily using standard finite element method (FEM) software. Once $\mathbf{u}(\mathbf{x})$ is determined, the distribution of cloak material properties can be obtained through Eq. (5).

For illustration, we consider an elliptical PM cloak immersed in the background water characterized by $\rho_0 = 1000$ kg/m^3 and $K_0 = 2.25$ GPa [13]. The half-long and half-short axes of the cloak shell are 2m and 1.6m, respectively. The radius of the inner cavity is $b = 1$ m, and the radius of tiny void in the virtual space is $\delta = 10^{-3}$ m. In solving the quasi-curl-free $\mathbf{u}$ via Eq. (7), $\xi = 10^{-4}$ is used and Lamé constants are chosen as $\lambda =$ -1.9999 Pa and $\mu = 1$ Pa [22]. Firstly, the symmetry deviation of **F** tensor derived from **u** field, which is quantified by F_{12} - F_{21}, is checked and shown in Fig. 2a. It is seen the **F** tensor is overall very symmetric, the asymmetric part is lower than 10^{-3} in the most region and becomes a little bit larger only near the inner boundary. Safely, **S** tensor is defined using the symmetric part of **F**, i.e., $\mathbf{S}{=}(K_0/J)^{1/2}$ sym(**F**). Fig. 2b shows normalized density ρ/ρ_0 of the cloak shell, and it follows that $0<\rho/\rho_0<2$.

The symmetric **S** tensor can be diagonalized in its principal frame ($\mathbf{e}_n$, $\mathbf{e}_t$) as

$$\mathbf{S} = S_n \mathbf{e}_n \otimes \mathbf{e}_n + S_t \mathbf{e}_t \otimes \mathbf{e}_t, \tag{8}$$

$$S_{n,t} = \frac{1}{2}(S_{11} + S_{22} \mp h), \quad h = \sqrt{(S_{11} - S_{22})^2 + 4S_{12}^2}, \tag{9}$$

and the angle ϕ between the principal axis $\mathbf{e}_n$ and x axis (see Fig. 2c) is determined as

$$\tan\phi = 2S_{12}/(S_{11} - S_{22} - h). \tag{10}$$

The anisotropy of the PM modulus, i.e. the ratio of principal moduli S_t/S_n, and the principal orientation angle ϕ are the most important properties of the cloak for guiding wave around an obstacle, and they are contoured in Fig. 2c and 2d, respectively. It is seen that unlike the cylindrical case, the principal orientation is not axisymmetrically distributed and possesses a complex pattern. Fig. 2d shows the S_t/S_n contour, from which it is seen that the PM anisotropy is high and varies sharply near the inner boundary, and actually the anisotropy is also not distributed regularly. Since there is no symmetry in the PM pattern can be utilized, the microstructure design and assembly of non-circular cloak have to be done cell by cell, calling for a smarter and more automatic design scheme.

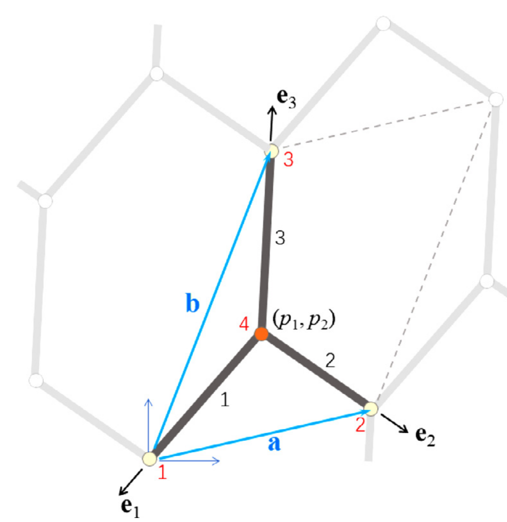

Fig. 3. Distorted honeycomb truss lattice model of PM.

Truss based PMs with honeycomb lattice

The required PM properties of the cloak can be realized with distorted honeycomb truss lattices as shown in Fig. 3, in which all bars are ideally hinged. A unit cell defined by lattice vectors $\mathbf{a} = (a_1, a_2)^T$ and $\mathbf{b} = (b_1, b_2)^T$ is indicated by the dashed parallelogram. The unit cell includes three bars characterized by tension stiffness E_iA_i and density ρ_i, where E_i and A_i are the Young's modulus and the section area of the bar i, respectively. Bar geometry is defined by nodes (1~3) on the lattice sites and one internal node 4. Without loss of generality, place the coordinate origin at the node 1, the node positions are then

$$\mathbf{r}_1=\mathbf{0},\quad \mathbf{r}_2=\mathbf{a},\quad \mathbf{r}_3=\mathbf{b},\quad \mathbf{r}_4=\mathbf{p}=\begin{pmatrix}p_1\\p_2\end{pmatrix}. \tag{11}$$

In microstructure design and assembling stage, suppose that the cloak domain is divided into many quadrilateral cells, three bars should be embedded into each cell and the internal node will be precisely adjusted to meet the conditions for S_t/S_n and the principal orientation angle ϕ corresponding to the cell location.

As shown in Fig. 3, we define three unit vectors along each bar

$$\mathbf{e}_1=-\frac{\mathbf{p}}{l_1},\quad \mathbf{e}_2=\frac{\mathbf{a}-\mathbf{p}}{l_2},\quad \mathbf{e}_3=\frac{\mathbf{b}-\mathbf{p}}{l_3}, \tag{12}$$

where $l_1=|\mathbf{p}|$, $l_2=|\mathbf{a}-\mathbf{p}|$, $l_3=|\mathbf{a}-\mathbf{p}|$ are the bar lengths. Under any loading, tension forces $\mathbf{t}=(t_1,t_2,t_3)^{\mathrm{T}}$ in the three bars cannot be arbitrary and their relative ratios have to balance at node 4 in absence of external load [10], i.e., $t_1\mathbf{e}_1+t_2\mathbf{e}_2+t_3\mathbf{e}_3=0$, or equivalently

$$\frac{t_2}{l_2}\mathbf{a}+\frac{t_3}{l_3}\mathbf{b}=\left(\frac{t_1}{l_1}+\frac{t_2}{l_2}+\frac{t_3}{l_3}\right)\mathbf{p}. \tag{13}$$

Therefore, the final bar tensions can be expressed as

$$\mathbf{t}=\alpha\mathbf{s}=\alpha(s_1,\ s_2,\ s_3)^{\mathrm{T}}, \tag{14}$$

where coefficient α is to be determined and $\mathbf{s}$ can be solved via Eq. (13):

$$s_2=l_2\frac{p_2b_1-p_1b_2}{a_2b_1-a_1b_2},\quad s_3=l_3\frac{p_1a_2-p_2a_1}{a_2b_1-a_1b_2},\quad s_1=l_1\left(1-\frac{s_2}{l_2}-\frac{s_3}{l_3}\right). \tag{15}$$

The $\mathbf{s}$ vector is called self-stress state of the truss lattice subjected to periodic boundary. It represents also the non-compatible bar elongations which cannot be generated by nodal displacements [25]. The macroscopic stress is defined by integrating equilibrated microscopic stress $\boldsymbol{\sigma}$ over the cell domain Ω. Using the identity $\nabla\cdot(\mathbf{r}\otimes\boldsymbol{\sigma})=\boldsymbol{\sigma}$ in absence of body forces, the macroscopic stress is defined via tractions on the cell boundary $\partial\Omega$, which in this case of truss lattice is just a sum including the forces $t_1\mathbf{e}_1$, $t_2\mathbf{e}_2$ and $t_3\mathbf{e}_3$:

$$\boldsymbol{\Sigma}=\frac{1}{V_{\text{cell}}}\int_\Omega\boldsymbol{\sigma}\mathrm{d}\mathbf{r}=\frac{1}{V_{\text{cell}}}\int_{\partial\Omega}\mathbf{r}\otimes(\boldsymbol{\sigma}\cdot\mathbf{n})\mathrm{dA}=\frac{1}{V_{\text{cell}}}\sum_{n=1}^{3}\mathbf{r}_n\otimes(t_n\mathbf{e}_n). \tag{16}$$

where V_{cell} is the area of unit cell. Substituting Eqs. (11), (12) and (14) in to Eq. (16), it can be shown that $\boldsymbol{\Sigma}$ depends only on the internal node position (p_1,p_2) and the undetermined coefficient α,

$$\boldsymbol{\Sigma}(p_1,\ p_2,\ \alpha)=\frac{\alpha}{V_{\text{cell}}}\bar{\mathbf{S}}(p_1,\ p_2), \tag{17}$$

where:

$$\begin{aligned}&\bar{\mathbf{S}}(p_1,\ p_2)=\tfrac{s_2}{l_2}\mathbf{a}\otimes\mathbf{a}+\tfrac{s_3}{l_3}\mathbf{b}\otimes\mathbf{b}-\mathbf{p}\otimes\mathbf{p}\\&=s_1l_1\mathbf{e}_1\otimes\mathbf{e}_1+s_2l_2\mathbf{e}_2\otimes\mathbf{e}_2+s_3l_2\mathbf{e}_3\otimes\mathbf{e}_3.\end{aligned} \tag{18}$$

To determine the unknown α under macroscopic strain $\mathbf{E}$, suppose the bars undergo firstly an affine elongation $\mathbf{e}^{\text{aff}}=(e_1^{\text{aff}},\ e_2^{\text{aff}},\ e_3^{\text{aff}})^{\mathrm{T}}$, where

$$e_b^{\text{aff}}=l_b(\mathbf{e}_b\cdot\mathbf{E}\cdot\mathbf{e}_b)=l_b(\mathbf{e}_b\otimes\mathbf{e}_b):\mathbf{E},\quad b=1\sim3. \tag{19}$$

Bar tension induced by affine elongations are not balanced, therefore $\mathbf{e}^{\text{aff}}$ must be relaxed by an extra $\Delta\mathbf{e}$ to reach the true elongations, i.e.

$$\mathbf{e}^{\text{aff}}+\Delta\mathbf{e}=\mathbf{e}=\alpha\begin{pmatrix}\frac{s_1l_1}{E_1A_1} & \frac{s_2l_2}{E_2A_2} & \frac{s_3l_3}{E_3A_3}\end{pmatrix}^{\mathrm{T}}. \tag{20}$$

Since $\Delta\mathbf{e}$ is compatible, it must not overlap with the non-compatible elongation $\mathbf{s}$, that is, $\mathbf{s}^{\mathrm{T}}(\mathbf{e}-\mathbf{e}^{\text{aff}})=\mathbf{0}$, with which it can be solved that

$$\begin{aligned}\alpha&=\bar{k}(s_1l_1\mathbf{e}_1\otimes\mathbf{e}_1+s_2l_2\mathbf{e}_2\otimes\mathbf{e}_2+s_3l_3\mathbf{e}_3\otimes\mathbf{e}_3):\\ \mathrm{E}&=\bar{k}(\bar{\mathbf{S}}{:}\mathbf{E}),\end{aligned} \tag{21}$$

where

$$\bar{k}=\left(\frac{s_1^2l_1}{E_1A_1}+\frac{s_2^2l_2}{E_2A_2}+\frac{s_3^2l_2}{E_3A_3}\right)^{-1}. \tag{22}$$

Combining Eqs. (17) and (21) gives

$$\boldsymbol{\Sigma}=\frac{\bar{k}(\bar{\mathbf{S}}:\mathbf{E})}{V_{\text{cell}}}\bar{\mathbf{S}}=(\mathbf{S}\otimes\mathbf{S}):\mathbf{E}, \tag{23}$$

where

$$\mathbf{S}(p_1,\ p_2)=\sqrt{\frac{\bar{k}}{V_{\text{cell}}}}\bar{\mathbf{S}}, \tag{24}$$

is just the characteristic stress tensor of PM as required by Eq. (5). In the inverse design, given a unit cell specified by vectors (**a, b**) as well as desired S_t/S_n and angle ϕ, the internal node location (p_1, p_2) can be conveniently solved out using Eqs. (9), (10), (15) and (18). Then the density $\rho=(\Sigma\rho_il_iA_i)/V_{\text{cell}}$ and the absolute magnitude of $\mathbf{S}$ will be matched by ρ_i and E_iA_i of bars. In the following, for the three bars in the same cell indexed by c, bar properties are set as the same $E_iA_i=E_cA_c$ and $\rho_i=\rho_c$.

Design and validation of integral latticed cloak

In order to build the cloak with an assemblage of graded PM lattices, the cloak region needs to be reasonably meshed into a set of cells which is inevitably non-uniform, then for each cell a three-bar PM model can be appropriately designed and housed according to the previous section. Due to the mirror symmetry, the procedure is illustrated by a quarter of the cloak shown in Fig. 4. At first, a quasi-conformal mesh lines are generated using an algorithm described in the following, so as the cloak region is divided into an almost rectangle mesh with reasonable mesh density, as shown in Fig. 4a. Second, the midpoints of rectangular edges are used as vertices to general whole set of rhombic cells which will be as regular as possible (Fig. 4b), then the PM design procedure given in the previous section can be executed repeatedly for each rhombic PM cell. Third, for each PM cell c, corresponding vectors ($\mathbf{a}_c$, $\mathbf{b}_c$) and $\mathbf{S}(\mathbf{x}_c)$ are then obtained with $\mathbf{x}_c$ being the cell center, thus the internal node location as well as the bar properties (E_cA_c, ρ_c) can be solved. This design procedure for the integral latticed cloak has been automated by appropriate programming.

The algorithm for producing meshes in Fig. 4a is borrowed from Ref. [26], which is originally developed for building quasi-conformal coordinate mapping for arbitrary geometry. In accordance with the elliptical shell, suppose that the mesh are specified by a set of circumferential grid lines $r(x,y)=r_m$, $(m=1{\sim}m_c)$, and a set of radial grid lines $\theta(x,y)=\theta_n$, $(n=1{\sim}n_c)$, as selectively exemplified in red and blue in Fig. 4a. The functions r and θ can be obtained by solving Laplace equations $\nabla^2r=0$ and $\nabla^2\theta=0$ on the quarter cloak domain, with appropriate applied boundary constraints. In particular, for $r(x,y)$:

Dirichlet condition $r=0$ on ∂D, $r=1$ on ∂B,
Neumann condition $\mathbf{n}\cdot\nabla r=0$ on ∂A and ∂C;

while for $\theta(x,y)$:

Dirichlet condition $\theta=0$ on ∂A, $\theta=\pi/2$ on ∂C
Neumann condition $\mathbf{n}\cdot\nabla\theta=0$ on ∂B and ∂D.

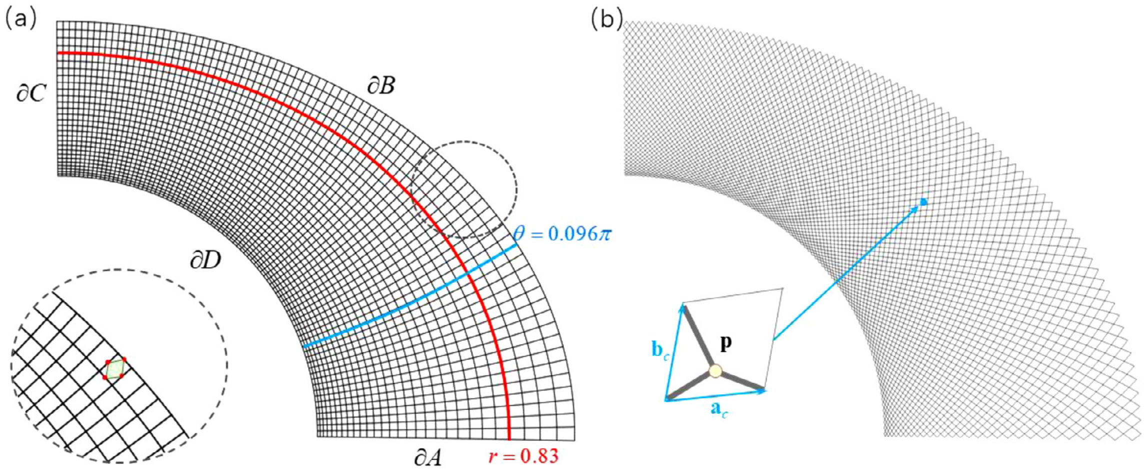

Fig. 4. Procedure of cloak design with truss lattice: **a** Generation of quasi-quadrilateral mesh; **b** Gradient rhombic cells for housing the three-bar PM model.

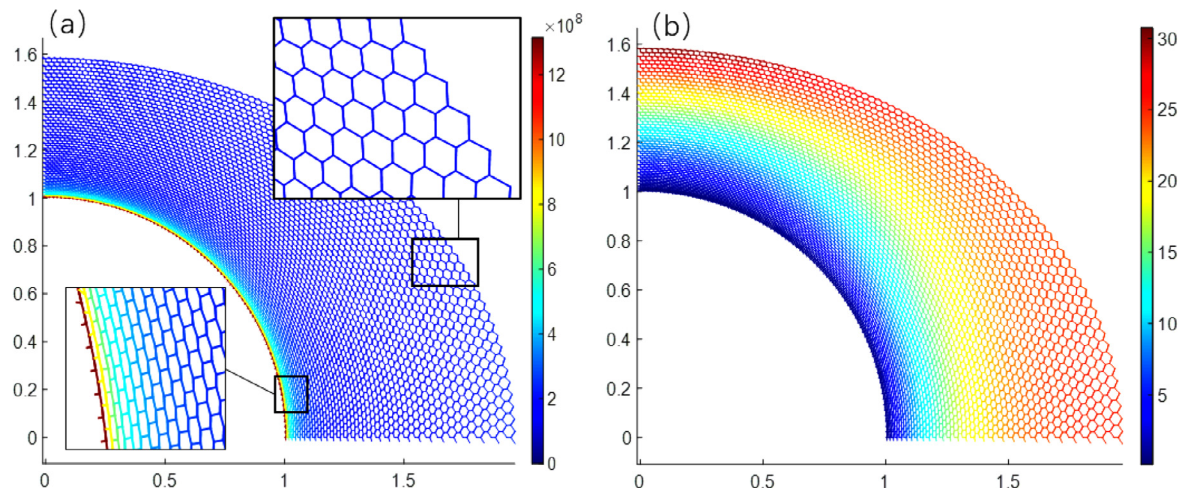

Fig. 5. Configuration and parameters of latticed cloak: **a** Color plot of bar stiffness EA; **b** Color plot of line density ρA of bars.

Here $\mathbf{n}$ is the unit normal vector on domain boundary. The physical meaning of this boundary conditions is that: bounded by $r \in [0, 1]$, i.e. ∂B and ∂D, $r = r_m$ grid lines are equipotential lines ruled by the Laplace equation, but the ends of grid line are allowed to slide along ∂A and ∂C in order to be orthogonal to them. Similar explanation applies to the θ lines. The Laplace equation together with the proposed boundary condition is actually equivalent to minimization of the Winslow functional which keeps the grid lines as mutually orthogonal as possible [26]. The scheme is quite general can be used to automatically generate for irregular domain a regular mesh division, so as to ease the PM design stage. In Fig. 4a, $m_c = 29$ circumferential grid lines and $n_c = 84$ radial grid lines are used to mesh the cloak, and lines of $r = 0.83$ and θ=0.096π are highlighted. The discrete r_m and θ_n values can be adjusted to control the mesh density, e.g. that, denser division is desired where material properties possess high gradient.

Finally, the design of cloak lattice realizing the previously determined material distribution in Fig. 2 is completed and displayed in Fig. 5. The colors in Fig. 5a and 5b indicate tension stiffness EA and line density ρA of bars, respectively. There are totally 4358 PM cells in a quarter of the cloak. The zoomed view of Fig. 5a details the gradually changed irregular honeycomb lattice, which is irregularly distorted and very different with an axisymmetric circular cloak.

In order to check the wave concealing performance of the designed cloak, full wave simulation is performed using commercial FEM software ANSYS, and the results are presented in Fig. 6. Figure 6a shows the pressure field in the background water when the immersed cloak lattice is illuminated by sound wave excited by a monopole acoustic point source placed upper left, and the operation frequency is 2.25 kHz. In the calculation, a fluid-structure interface is used to deal with bridging of the lattice bars and the acoustic fluid, while non-reflecting condition is set at the external boundary of background water. For comparison, Fig. 6b and 6c display the pressure fields of an un-cloaked void obstacle and a void protected by continuum cloak (with the material distribution described by Fig. 2), respectively, under the same wave loading. Inside the cloak shell of Fig. 6c, pseudo pressure $p = -J\sigma_{11}/\mathrm{F}_{11}$ is displayed instead. It is observed that, though the discretization of continuously varied material property and the approximation of PM by truss lattice bring a certain amount of error, the pressure fields of Fig. 6a and 6c exhibit high similarity. The scattering in case of the lattice cloak is significantly reduced, and the wave front passed through the target remains almost unperturbed as shown in Fig. 6a. Conversely in Fig. 6b, obvious reverberation and shadow are observed in case of a bare obstable. An advantage of PM cloak is its broadband effectivity since the metamaterial mechanism is not resonance based. As long as quasi-static homogenization is justified under the wavelength of the operating frequency, the cloak will work well. We conducted a supplementary simulation at a higher frequency 3.25 kHz, and the corresponding results are plotted in Fig. 6d, 6e and 6f for case of latticed cloak, bare obstacle

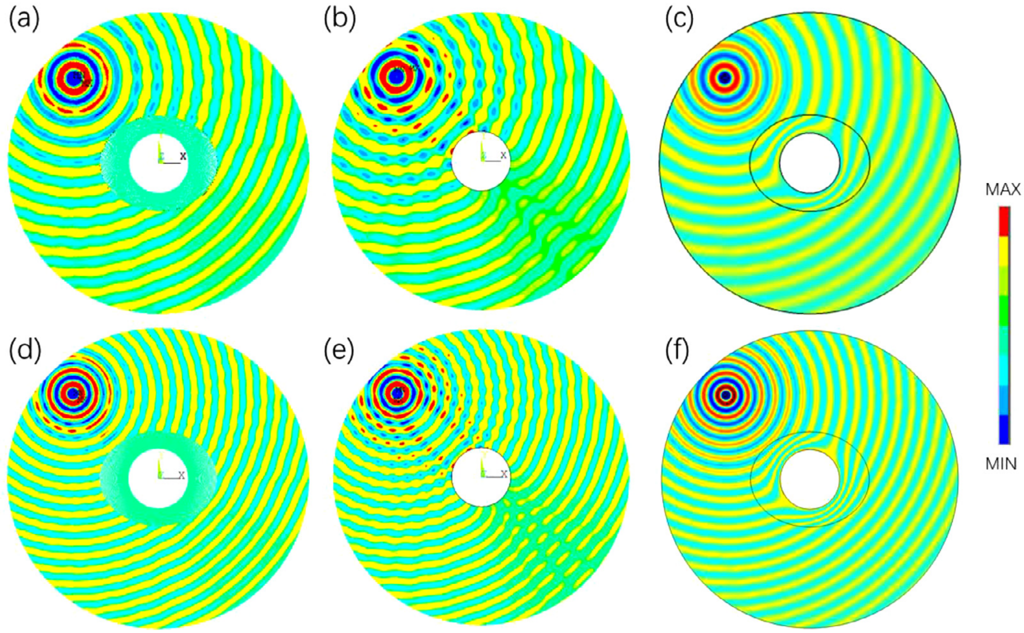

Fig. 6. Simulated pressure fields for different cases at frequency 2.25 kHz: **a** Latticed cloak; **b** Bare void; **c** Continuum cloak, and at frequency 3.25 kHz; **d** Latticed cloak; **e** Bare void; **f** Continuum cloak.

and continuum cloak, respectively, and as expected good cloaking performance is observed as well.

In summary, in this work, we have developed a complete set of techniques necessary for design of truss-based PM acoustic devices with irregular shape, including the analytical homogenization of PM for a general unit cell, its inverse design scheme, and algorithms for assembling the PM cells into a graded lattice representing a domain induced by PM transformation acoustics. The developed methods were gone through by the design of latticed elliptical PM cloak for the first time, and effectiveness was numerically validated by the well wave concealing performance. The work proves that, together with the algorithm of numerical quasi-curl-free coordinate mapping [22], more general PM underwater acoustic wave devices beyond the simple geometry can be expected to be brought into reality. Of course, the ideal truss model used here is still very theoretical, and it is noticed that the bar parameters and lattice discretization here is very stringent. More future works, including optimization and compromise between the cloaking performance and material sharpness as well as the feasible continuum-based PM design are in order to put them forward to experimental demonstration.

Declaration of Competing Interest

The authors declare that they have no known competing financial interests or personal relationships that could have appeared to influence the work reported in this paper.

Acknowledgments

This work was supported by the National Natural Science Foundation of China (Grant Nos. 11972080, 11972083 and 11991030) and the Innovation Foundation of Maritime Defense Technologies Innovation Center (Grant No. JJ-2021-719-06).

References

[1] J.B. Pendry, D. Schurig, D.R. Smith, Controlling electromagnetic fields, Science 312 (2006) 1780–1782.
[2] U. Leonhardt, Optical conformal mapping, Science 312 (2006) 1777–1780.
[3] L.S. Dolin, To the possibility of comparison of three-dimensional electromagnetic systems with non-uniform anisotropic filling (in Russia), Izv. Vyssh. Uchebn. Zaved. Radiofiz. 4 (1961) 964–967.
[4] D. Schurig, J.J. Mock, B.J. Justice, et al., Metamaterial electromagnetic cloak at microwave frequencies, Science 314 (2006) 977–980.
[5] S.A. Cummer, D. Schurig, One path to acoustic cloaking, N. J. Phys. 9 (2007) 45.
[6] H.Y. Chen, C.T. Chan, Acoustic cloaking in three dimensions using acoustic metamaterials, Appl. Phys. Lett. 91 (2007) 183518.
[7] D. Torrent, J. Sanchez-Dehesa, Anisotropic mass density by radially periodic fluid structures, Phys. Rev. Lett. 105 (2010) 430117.
[8] B.I. Popa, W. Wang, A. Konneker, et al., Anisotropic acoustic metafluid for underwater operation, J. Acoust. Soc. Am. 139 (2016) 3325.
[9] B. Popa, L. Zigoneanu, S.A. Cummer, Experimental acoustic ground cloak in air, Phys. Rev. Lett. 106 (2011) 253901.
[10] G.W. Milton, A.V. Cherkaev, Which elasticity tensors are realizable? ASME. J. Eng. Mater. Technol. 117 (1995) 483–493.
[11] C.N. Layman, C.J. Naify, T.P. Martin, et al., Highly anisotropic elements for acoustic pentamode applications, Phys. Rev. Lett. 111 (2013) 24302.
[12] M. Kadic, T. Bückmann, R. Schittny, et al., On anisotropic versions of three-dimensional pentamode metamaterials, New J. Phys. 15 (2013) 023029.
[13] Y. Chen, X.N. Liu, G.K. Hu, Latticed pentamode acoustic cloak, Sci. Rep. 5 (2015) 15745.
[14] A.N. Norris, Acoustic cloaking theory, Proc. R. Soc. A. 464 (2008) 2411–2434.
[15] Y. Chen, M. Zheng, X. Liu, et al., Broadband solid cloak for underwater acoustics, Phys. Rev. B. 95 (2017) 180104.
[16] S. Zhaoyong, J. Han, C. Yi, et al., Design of an underwater acoustic bend by pentamode metafluid, J. Acoust. Soc. Am. 143 (2018) 1029.
[17] Y. Chen, G. Hu, Broadband and high-Transmission metasurface for converting underwater cylindrical waves to plane waves, Phys. Rev. Appl. 12 (2019) 044046.
[18] A. Zhao, Z. Zhao, X. Zhang, et al., Design and experimental verification of a water-like pentamode material, Appl. Phys. Lett. 110 (2017) 011907.
[19] Y. Chen, X.N. Liu, P. Xiang, et al., Pentamode material for underwater acoustic wave control (in Chinese), Advances in Mechanics 46 (2016) 201609.
[20] L. Ning, Y.Z. Wang, Y.S. Wang, Active control cloak of the elastic wave metamaterial, Int. J. Solids Struct. 202 (2020) 126–135.
[21] L. Ning, Y.Z. Wang, Y.S. Wang, Broadband square cloak in elastic wave metamaterial plate with active control, J. Acoust. Soc. Am. 150 (2021) 4343–4352.
[22] Y. Chen, X. Liu, G. Hu, Design of arbitrary shaped pentamode acoustic cloak based on quasi-symmetric mapping gradient algorithm, J. Acoust. Soc. Am. 140 (2016) L405–L409.
[23] D.E. Quadrelli, G. Cazzulani, S. La Riviera, et al., Acoustic scattering reduction of elliptical targets via pentamode near-cloaking based on transformation acoustics in elliptic coordinates, J. Sound Vib. 512 (2021) 116396.
[24] H.L. Fan, W. Yang, Development of lattice materials with high specific stiffness and strength (in Chinese), Adv. Mech. 37 (2007) 99–112.
[25] S. Pellegrino, Structural computations with the singular-value decomposition of the equilibrium matrix, Int. J. Solids Struct. 30 (1993) 3025–3035.
[26] Z. Chang, X.M. Zhou, J. Hu, et al., Design method for quasi-isotropic transformation materials based on inverse Laplace's equation with sliding boundaries, Opt. Express 18 (2010) 6089–6096.